contrary to the trend shown by the geometric albedos of JII, JIII, and JIV. The satellite reflectivities are consistent only with a process that links decreasing absorption intensity to decreasing albedo. Another such process, geometrically analogous to the one described above, is the mixing of dark, nonfrost materials with the frost on the satellites' surfaces.

We note that as we move out in the satellite system from JII, not only do the absorption intensities decrease, the overall slopes of the satellite reflectivities change from albedo decreasing to albedo increasing with wavelength. This is consistent with a partial surface cover model in which the underlying material is a silicate, since almost all silicates show albedos increasing with wavelength (*21, 23*).

Satellite JI has anomalous characteristics that do not allow it to fit readily into the above discussion. Its infrared spectrum resembles that of JIV, but it is almost three times more reflective than JIV in the visible. The high visible reflectivity of JI suggests that it is extensively frost covered, but the absence of strong absorptions in its infrared reflectivity indicates that, if frost is present, the particles are much smaller than those on JII and JIII. Small frost particles might be produced from the disruption of larger particles by electrons from the high flux around JI (*25*). Charged particle radiation acting on impurities, such as sulfides, in a frost on JI might also explain its ultraviolet-visible absorption (*22, 24*). Laboratory measurements of the reflectivities of pure and impure frosts struck by charged particles would be useful in examining such a model.

Veverka (*26*) also suggested that charged particle radiation has altered the infrared reflecting characteristics of JI. He concluded from polarization measurements that snow predominates on the surfaces of JI, JII, and JIII, and rock predominates on the surface of JIV; this is consistent with our conclusions for JII, JIII, and JIV, based on their infrared reflectivities.

Figure 2 shows the infrared reflectivities of the leading and trailing sides of JIII, scaled to the same value at 5625 cm^{-1}. The water frost absorptions on the leading side are deeper, the intensity difference indicating a 20 percent greater frost cover. This is in good quantitative agreement with the observed 15 percent brightness difference between the two sides (*15, 22*). Since the leading and trailing sides of JII differ in brightness by 30 percent (*15, 22*), JII may show a greater absorption intensity difference between its two sides than JIII. A single observation of the trailing side of JI, not presented here, shows a stronger increase in reflectivity with wavelength than on the leading side and a maximum near 5000 cm^{-1}. More data for both sides should be obtained for all the satellites.

CARL B. PILCHER

Department of Chemistry and Planetary Astronomy Laboratory, Department of Earth and Planetary Sciences, Massachusetts Institute of Technology, Cambridge 02139

STEPHEN T. RIDGWAY

Kitt Peak National Observatory, Tucson, Arizona 85717, and Department of Physics, State University of New York, Stony Brook 11790

THOMAS B. MCCORD

Planetary Astronomy Laboratory, Massachusetts Institute of Technology

References and Notes

1. G. P. Kuiper, in *Atmospheres of the Earth and Planets* (Univ. of Chicago Press, Chicago, ed. 2, 1952), p. 340.
2. T. B. McCord, T. V. Johnson, J. H. Elias, *Astrophys. J.* **165**, 413 (1971).
3. C. B. Pilcher, C. R. Chapman, L. A. Lebofsky, H. H. Kieffer, *Science* **167**, 1372 (1970).
4. G. P. Kuiper, D. P. Cruikshank, U. Fink, *Sky Telesc.* **39**, 14 (1970).
5. G. P. Kuiper, in *Planets and Satellites*, G. P. Kuiper and B. M. Middlehurst, Eds. (Univ. of Chicago Press, Chicago, 1961), vol. 3, p. 305.
6. V. I. Moroz, *Sov. Astron. AJ* **9**, 999 (1966).
7. H. Kieffer, *J. Geophys. Res.* **75**, 501 (1970); thesis, California Institute of Technology (1968).
8. ———, personal communication.
9. L. Gromova, V. I. Moroz, D. P. Cruikshank, *Astron. Circ.* **569**, 6 (1970).
10. T. V. Johnson and T. B. McCord, *Astrophys. J.* **169**, 589 (1971).
11. D. Morrison and D. P. Cruikshank, in preparation.
12. J. S. Lewis, *Icarus* **15**, 174 (1971).
13. H. L. Johnson, I. Coleman, R. I. Mitchell, D. L. Steinmetz, *Commun. Lunar Planet. Lab.* **7**, 83 (1968).
14. T. B. McCord and T. V. Johnson, *Science* **169**, 855 (1970).
15. D. L. Harris, in *Planets and Satellites*, G. P. Kuiper and B. M. Middlehurst, Eds. (Univ. of Chicago Press, Chicago, 1961), pp. 291–293.
16. J. Stebbins and T. S. Jacobsen, *Lick Obs. Bull. No. 401* (1928).
17. B. T. O'Leary, paper presented at the 4th annual meeting of the Division of Planetary Sciences of the American Astronomical Society, Kona, Hawaii, March 1972.
18. P. Fellgett, thesis, University of Cambridge (1951).
19. G. P. Kuiper, D. P. Cruikshank, U. Fink, *Bull. Amer. Astron. Soc.* **2**, 235 (1970).
20. F. C. Gillett, K. M. Merrill, W. A. Stein, *Astrophys. Lett.* **6**, 247 (1970).
21. J. A. Adams and A. L. Filice, *J. Geophys. Res.* **72**, 5705 (1967).
22. T. V. Johnson, *Icarus* **14**, 94 (1971); thesis, California Institute of Technology (1969).
23. G. R. Hunt and J. W. Salisbury, *Mod. Geol.* **1**, 283 (1970).
24. T. V. Johnson and T. B. McCord, *Icarus* **13**, 37 (1970).
25. P. Goldreich and D. Lynden-Bell, *Astrophys. J.* **156**, 59 (1969).
26. J. F. Veverka, *Icarus* **14**, 355 (1971).

27. One of us (C.B.P.) was a visiting astronomer at Kitt Peak National Observatory. The observatory is operated by the Association of Universities for Research in Astronomy for the National Science Foundation. We thank H. Kieffer for allowing us to use his water frost spectrum prior to its publication as well as for many helpful discussions. C. Chapman reviewed the manuscript and made many useful suggestions. Helpful discussions were also held with T. Johnson and C. Reisz. The Idealab Fourier spectrometer was made available to us by the Astronomy Program of the State University of New York, Stony Brook. This work was supported in part by an NSF grant to the State University of New York, Stony Brook, and NASA grant NGR 22-009-473. Contribution No. 64 from the Planetary Astronomy Laboratory, Department of Earth and Planetary Sciences, Massachusetts Institute of Technology. Send correspondence to C.B.P.

15 September 1972

Internal Gravity Wave–Atmospheric Wind Interaction: A Cause of Clear Air Turbulence

Abstract. *The interaction between an internal gravity wave and a vertical wind shear may be responsible for the production of clear air turbulence in the free atmosphere. A simplified model equation demonstrates the feasibility of the suggested mechanism.*

Clear air turbulence (CAT) consists of all turbulent motions in regions of the free atmosphere that are not close to visible convective activity. It not only menaces aviation, but is also important in atmospheric circulation. A review of scant observations of CAT (*1*) shows that it appears in sporadic patches of apparently stable atmospheric layers with vertical wind shear. When CAT occurs, spectral analyses of the atmospheric motions consistently exhibit a marked gap in the spectral energy density, $E(k)$ (*2*). The "spectral gap" is accompanied by an energy bulge at higher wave numbers. Various hypotheses have been advanced to explain the occurrence of CAT associated with this spectral energy bulge (*1*). It is often speculated that the most likely energy source for CAT is the shear present in large-scale wind structure, which leads to Kelvin-Helmholtz instability (*3*, p. 481) and thus causes turbulence production. Theoretical studies (*4*) have shown that such an instability can occur only when the gradient Richardson number

$$\mathrm{Ri} = (-g/\bar{\rho})(d\bar{\rho}/dz)(\partial\bar{U}/\partial z)^{-2}$$

is less than ¼. (Here, g is the gravitational acceleration, $\bar{\rho}$ is the mean density, $\bar{U}$ is the mean wind velocity, and z is the altitude.) This agrees qualitatively with Richardson's criterion (*5*, p. 381), a sufficient condition to ensure the destruction of any existing turbulence. The relevance of the presence of internal gravity waves (IGW's) to CAT has been mentioned frequently (*1*, *6*), but usually without specific discussion of the important physical processes. In this report we present a mechanism of wind shear enhancement and Ri reduction in localized patches of the atmosphere as a consequence of the interaction between a traveling IGW and a mean flow of appropriate horizontal velocity. Thus, with an initially stable atmosphere (Ri greater than ¼), an IGW-wind interaction could cause the growth of atmosphere turbulence.

The interaction of IGW's and wind shear at a critical level, where the horizontal phase velocity of the propagating IGW has null value relative to the local horizontal atmospheric mean flow, has been investigated (*7*) for IGW's in an inviscid Boussinesq fluid (*3*, p. 16) with a continuous shear flow. It has been shown that, as the wave passes through its critical level, z_c, it is attenuated by a factor $\exp(-2\pi\mu)$, where $\mu = [\mathrm{Ri}(z_c) - \frac{1}{4}]^{\frac{1}{2}}$. The Reynolds stress of a wave propagating upward is given (*7*) by

$$\overline{u_0'w_0'} = c\mu|A|^2k^{-1}$$

where u_0' and w_0' are the horizontal and vertical components of the fluid motion associated with the IGW, k is the horizontal component of the wave number vector, A is a measure of the amplitude of the IGW well below the critical level of interaction, and $c = \frac{1}{2}\exp(2\pi\mu)$ if $z < z_c$, or $c = -\frac{1}{2}$ if $z > z_c$. The extension (*8*) to include the effects of viscosity, ν, give a finite thickness for the critical layer of the order of the characteristic length,

$$z_0 = \nu^{1/3}(k\partial\bar{U}/\partial z)^{-1/3}$$

The Reynolds stress of the internal gravity wave decreases almost linearly within the critical layer, as shown in Fig. 1.

To circumvent the mathematical difficulty of treating the development of an IGW-wind interaction, we derived (*9*) a model equation from the perturbed nonlinear Navier-Stokes equations (*10*, p. 13) by taking a horizontal spatial average over a wavelength of the IGW. Thus, the model equation of interaction reflects the mean momentum conservation for a volume element having its horizontal dimension equal to a wavelength. The atmosphere is assumed to be isothermal and incompressible so that the Boussinesq approximation holds (*3*, p. 16) and to have initially a horizontal mean wind, $\bar{U}(z)$. The x-axis of the coordinate system aligns with the horizontal component of the propagation wave number vector of the traveling monochromatic IGW (see Fig. 2). Inasmuch as ambient turbulence is allowed, we let the velocity be

$$u(x,z,t) = \bar{U}(z,t) + u_0'(x,z,t) + u_1'(x,z,t)$$
$$w(x,z,t) = w_0'(x,z,t) + w_1'(x,z,t)$$

where u_0' and w_0' denote the horizontal and vertical components of the fluctuating motion associated with the IGW, u_1' and w_1' the components of the turbulent fluctuation, and t the time. In the turbulence-free case, the velocity reduces to that given in (*7*, *8*). Consider the case that the wave and turbulent motions have a negligible correlation, which is appropriate when their scale sizes are quite different. The substitution of the velocity components described above into the Navier-Stokes equations for a stratified fluid with the usual simplifications for the derivation of the Reynolds equation (*10*, p. 13) results in the model equation

$$\frac{\partial\bar{U}}{\partial t} + \frac{\partial}{\partial z}\overline{(u_1'w_1')} - \nu\frac{\partial^2\bar{U}}{\partial z^2} = -\frac{\partial}{\partial z}\overline{(u_0'w_0')} \quad (1)$$

where spatial averages are used rather than the customary temporal averages. The viscous shear stress in Eq. 1 is generally negligible compared to the "apparent" shear stress due to turbulence. The gradient Reynolds stress, the second term on the left side of the equation, represents the momentum transport, per unit mass, due to turbulent motion. Its counterpart on the right side is ascribed to that due to the wave motion. The net momentum transport accounts for the rate of change of the mean motion.

The momentum transport terms in Eq. 1 must be prescribed before the determination of $\bar{U}$. For the sake of simplicity, we follow Prandtl's mixing-length hypothesis (*10*, p. 277) to approximate the turbulent Reynolds stress

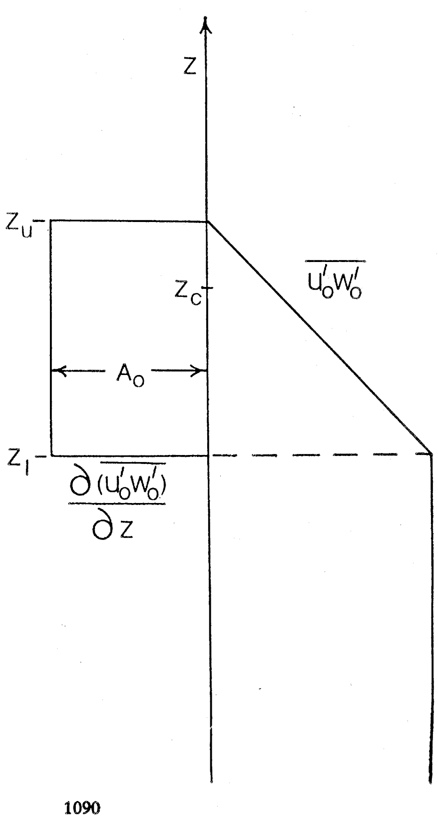

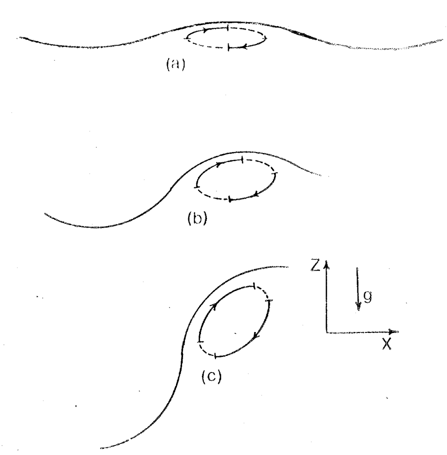

Fig. 1 (left). Model of Reynolds stress, $\overline{u_0'w_0'}$, and its gradient for an internal gravity wave; z_c is the critical level; z_u and z_l are the upper and lower limits of the critical layer; A_0 is defined by Eq. 2. Fig. 2 (right). Schematic diagram of the wave pattern and particle path with respect to the mean background flow (a) near z_c, (b) below z_c, but within the critical layer, and (c) below the critical layer.

term. The wave Reynolds stress term can be approximated by using a modification of the results that were discussed earlier (*8*). To the approximation of the mixing-length theory, the effects of turbulent mixing can be estimated by a reinterpretation of the kinematic viscosity. Replacing ν by the turbulent viscosity coefficient, ϵ, we obtain a turbulent length scale for the thickness of the critical layer,

$$z_1 = \epsilon^{1/3}\,[k\partial\bar{U}(z_c)/\partial z]^{-1/3}$$

In view of the earlier expression for $\overline{u_0'\,w_0'}$ (*7*), Eq. 1 becomes

$$\frac{\partial\bar{U}}{\partial t} - \epsilon\,\frac{\partial^2\bar{U}}{\partial z^2} = A_0 \qquad (2)$$

where

$$A_0 = \mu|A|^2(e^{2\pi\mu}+1)\,[2k(z_u - z_1)]^{-1}$$

if $z_1 < z < z_u$ and $A_0 = 0$ otherwise, $z_u = z_c + 2z_1$, and $z_1 = z_c - 5z_1$ (see Fig. 1). The left side of Eq. 2 is recognizable as a diffusion equation. The term on the right side can be treated as a momentum source representing the momentum transfer from the IGW to the background mean wind. The distortion of the structure of an upward propagating IGW near a critical layer is illustrated in Fig. 2. The momentum transfer mechanism of the IGW Reynolds stress can be seen as follows: As shown schematically in Fig. 2, on the average, parcels of fluid with a positive value of w_0' also have a positive value of u_0', and those with a negative value of w_0' also have a negative value of u_0', so that $\overline{u_0'w_0'} > 0$. This indicates a net upward transport of positive horizontal IGW momentum. Within the critical layer, $\overline{u_0'w_0'}$ decreases almost linearly (*8*) as the wave itself becomes more and more horizontal. (In Fig. 2, compare the proportions of the solid lines, $\overline{u_0'w_0'} > 0$, and the dashed lines, $\overline{u_0'w_0'} < 0$, as the wave progresses upward.) Therefore, the net momentum exchange within the critical layer accelerates the mean background flow in the direction of horizontal wave propagation (x-direction) and the mechanism results in regions of increased vertical shear. However, the turbulent Reynolds stress tends to nullify the existing mean velocity gradient. The quasi-steady distribution of the mean velocity near the critical level represents a balance between the rates of momentum absorption from the IGW and momentum transport due to the turbulence.

Since the term A_0 makes Eq. 2 nonlinear, an iterative numerical scheme is used for parametric analysis and solution. A sample of the results is shown in Fig. 3, where the origin ($z = 0$) is taken to be the initial location of the critical level and the wave-wind interaction is assumed to begin at $t = 0$. Representative values for the wave parameters and atmospheric flow properties in the lower stratosphere (10 to 12 km) were obtained from reports of experimental observations (*11*) and are indicated in Fig. 3 for the example given. The initial mean wind profile is assumed to be linear although this condition is not at all necessary. It can be seen in Fig. 3 that, as the IGW-wind interaction progresses, the critical level moves downward and $\partial\bar{U}/\partial z$ at the critical level increases. This results in a larger fraction of the wave momentum being able to pass through the critical layer without being absorbed and is reflected in reduced values of A_0 and $(z_u - z_1)$ after each iteration.

The results show that under certain typical conditions the interaction of an IGW with a background wind shear near a critical level provides a mechanism for depositing sufficient momentum in certain regions of the atmosphere to significantly increase the local mean

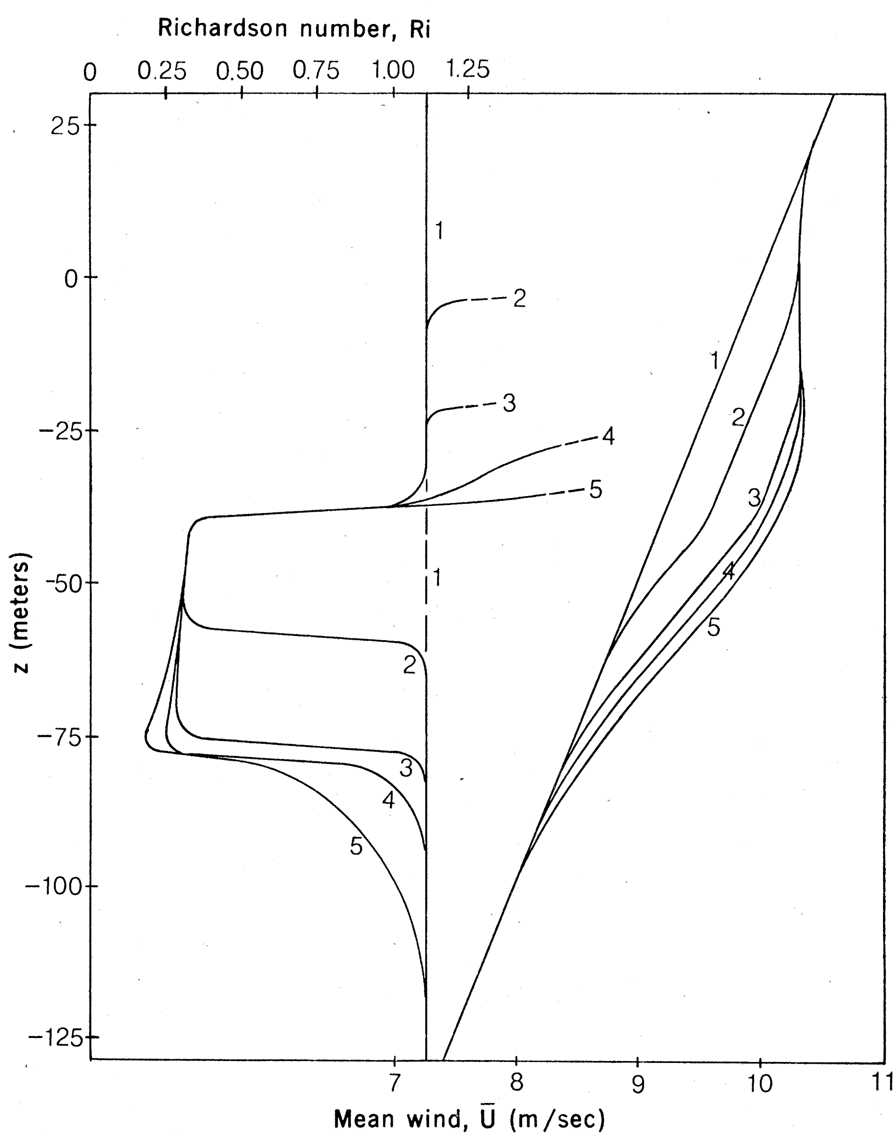

Fig. 3. Example of results when the initial ($t = 0$) location of the critical level ($z = z_c = 0$) corresponds to $\bar{U} = 10$ m/sec, $k = 1.26$ km^{-1}, $\overline{u_0'w_0'} = 0.1$ m^2/sec^2 at $z = -\infty$, $\partial\bar{U}/\partial z = 0.02$ sec^{-1} and Ri = 1.102 at $t = 0$, $[(-g/\bar{\rho})(d\bar{\rho}/dz)]^{1/2} = 0.021$ sec^{-1}, and $\epsilon = 0.1$ m^2/sec for (1) $t = 0$, (2) $t = 200$, (3) $t = 400$, (4) $t = 750$, and (5) $t = 10{,}000$ seconds. The critical Richardson number is 0.25.

wind shear. Since the interaction reduces Ri below ¼ over regions of the order of $(z_u - z_l)$ in vertical extent, it could cause turbulence to grow into patches of this thickness. The parameters that influence the interaction include the amplitude and horizontal wave number of the IGW, the initial background wind shear near the critical level, and the intensity of the ambient turbulence. The presence of a moderate intensity of ambient turbulence tends to prevent the catastrophic buildup in the mean wind shear that might cause severe CAT.

What has been described is undoubtedly not the only cause of CAT, but it does demonstrate that the interaction of IGW's with vertical wind shear can lead to the production of turbulence. The irregular occurrence of critical levels in apparently stable regions of the atmosphere is consistent with the observed patchy and intermittent nature of CAT. Although the interaction mechanism has been described here in relation to the lower stratosphere (for which observational data were available) the basic phenomenon is not expected to be restricted to this region. Furthermore, since salinity (and thus density) varies with depth in the ocean, IGW's exist there, and a similar mechanism for causing turbulence is likely to occur. A straightforward extension of the present theory could include the multichromatic IGW's that exist in a real atmosphere. The theory presented here appears worthy of experimental studies of its validity.

K. BEKOFSKE
V. C. LIU
Department of Aerospace Engineering, University of Michigan, Ann Arbor 48104

References and Notes

1. Y. H. Pao and A. Goldburg, Eds., *Clear Air Turbulence and Its Detection* (Plenum, New York, 1969).
2. N. K. Vinnichenko and J. A. Dutton, *Radio Sci.* **4**, 1115 (1969).
3. S. Chandrasekhar, *Hydrodynamic and Hydromagnetic Stability* (Oxford Univ. Press, London, 1961).
4. J. W. Miles, *J. Fluid Mech.* **10**, 496 (1961); L. N. Howard, *ibid.*, p. 509.
5. L. Prandtl, *Essentials of Fluid Dynamics* (Hafner, New York, 1952).
6. C. O. Hines, *J. Atmos. Terr. Phys.* **30**, 837 (1968); A. A. Townsend, *J. Fluid Mech.* **32**, 145 (1968).
7. J. R. Booker and F. P. Bretherton, *J. Fluid Mech.* **27**, 513 (1967).
8. P. Hazel, *ibid.* **30**, 775 (1967).
9. K. Bekofske, thesis, University of Michigan, in preparation.
10. J. O. Hinze, *Turbulence* (McGraw-Hill, New York, 1959).
11. D. N. Axford, *Quart. J. Roy. Meteorol. Soc.* **96**, 273 (1970); *ibid.* **97**, 313 (1971).
12. Supported in part by NASA grant NGR 23-005-094.

25 July 1972

Obsidian Trade Routes in the Mayan Area

Abstract. *Obsidian from two sources in highland Guatemala has been found at 23 sites of the Classic Mayan civilization, mainly in the nonvolcanic lowlands to the north. The distribution, together with trade routes suggested by topography and documentary sources, suggests efficient waterborne transport and competition between sources for the lowland market.*

Trace-element analysis of obsidians has been used recently in both the Middle East and Mesoamerica as a method of documenting prehistoric trade (*1*). Studies have been based on a large number of determinations, and a fairly accurate picture of the temporal and spatial limits of the distribution of any one source has been elucidated. In the Mayan area centered on Guatemala and the Yucatán only a few determinations have so far been reported for the Classic Mayan civilization of the 3rd to 9th centuries A.D., but these preliminary results can be used to construct a model explaining the distribution of obsidians in the Mayan area which may be tested by further analyses.

The Mayan area is divided into three parts: a southern highland zone, a central lowland with tropical rain-forest vegetation, and a northern lowland with tropical scrub vegetation. The highlands are volcanic and possess a number of known obsidian sources; the lowlands have a sedimentary limestone geology (except for the horst of the Maya Mountains) and lack obsidian. The contrasting geology and relief of the highlands and lowlands results in different ranges of environmental niches and available resources, and trade in a variety of commodities between the two zones in prehistoric times has been demonstrated (*2*, pp. 124–158).

Two major sources of obsidian exploited by the Classic Maya have been identified in the highlands (Fig. 1). One is at El Chayal, 20 km northeast of Guatemala City; the other is some 50 km to the southeast at Ixtepeque-Papalhuapa, near the modern town and Classic site of Asunción Mita, the southernmost major center of the lowland-based civilization.

Analysis by x-ray fluorescence has shown that obsidians from these two sources can be characterized and differentiated, especially on the basis of their ratio of Fe to Mn and Ti to Ba, the presence or absence of Sr and Ba, and, to some extent, the relative amounts of Zr, Sr, and Rb, although this has a high noise level (*3*).

On the basis of such analyses of obsidians from 23 Classic period sites, it is possible to attribute the obsidian to either the El Chayal or the Ixtepeque source (Fig. 1). El Chayal obsidian is found in the highlands to the west of the source, and in the lowlands in the Usumacinta River Basin, in northeastern Petén and the Belize Valley, and in the Toledo District of southern Belize (British Honduras). Ixtepeque obsidian is found east and north of the source (except for one sample of undated obsidian from Kaminaljuyú) along the Caribbean coast of Belize, in northeastern Petén and the Belize Valley, and in northern Yucatán.

The pattern of distribution of both sources is thus elongated northward from the source, from the volcanic highlands into the nonvolcanic lowlands where obsidian was desired for both utilitarian and ritual purposes. Lowland products were clearly sent in the other direction in exchange for obsidian and other highland goods. The exact routes involved in this trade have not been established, but evidence derived from topography, ethnohistory, and ethnography supplies a number of possibilities. Topography suggests that trade routes followed the river valleys: the Río Negro and the Río de la Pasión flow directly down to the lowlands, converging to form the Usumacinta; the Río Motagua flows northeast to the Caribbean, and the Río Grande, the Belize River, the Río Hondo, and the Sarstoon River flow from Petén east to the Caribbean.

Transport on these routes would be by porter to the head of navigation and then downstream by canoe to the sea. In Spanish documents of the early colonial period a number of overland routes are mentioned: from Chetumal Bay across the Yucatán to Uxmal and the sites around the Puuc Hills; from Ascension Bay on the coast of Quin-